Fibers and Polymers 2006, Vol.7, No.4, 389-397

A Three-dimensional Biomechanical Model for Numerical Simulation of Dynamic Pressure Functional Performances of Graduated Compression Stocking (GCS)

Rong Liu*, Yi-Lin Kwok, Yi Li, Terence-T Lao[1], Xin Zhang[2], and Xiao Qun Dai

Institute of Textiles and Clothing, The Hong Kong Polytechnic University, Hung Hom, Kowloon, Hong Kong
[1]Department of Obstetrics and Gynaecology, Faculty of Medicine, The University of Hong Kong, Queen Mary Hospital, Pokfulam Road, Hong Kong
[2]Department of Clothing Art and Design, Xi'an Polytechnic University, Xi'an, China
(Received May 16, 2006; Revised September 6, 2006; Accepted October 25, 2006)

Abstract: The beneficial effects of graduated compression stockings (GCS) in prophylaxis and treatment of venous disorders of human lower extremity have been recognized. However, their pressure functional performances are variable and unstable in practical applications, and the exact mechanisms of action remain controversial. Direct surface pressure measurements and indirect material properties testing are not enough for fully understanding the interaction between stocking and leg. A three-dimensional (3D) biomechanical mathematical model for numerically simulating the interaction between leg and GCS in dynamic wear was developed based on the actual geometry of the female leg obtained from 3D reconstruction of MR images and the real size and mechanical properties of the compression stocking prototype. The biomechanical solid leg model consists of bones and soft tissues, and an orthotropic shell model is built for the stocking hose. The dynamic putting-on process is simulated by defining the contact of finite relative sliding between the two objects. The surface pressure magnitude and distribution along the different height levels of the leg and stress profiles of stockings were simulated. As well, their dynamic alterations with time processing were quantitatively analyzed. Through validation, the simulated results showed a reasonable agreement with the experimental measurements, and the simulated pressure gradient distribution from the ankle to the thigh (100:67:30) accorded with the advised criterion by the European committee for standardization. The developed model can be used to predict and visualize the dynamic pressure and stress performances exerted by compression stocking in wear, and to optimize the material mechanical properties in stocking design, thus, helping us understand mechanisms of compression action and improving medical functions of GCS.

Keywords: Bio-mechanical model, Numerical simulation, Pressure functional performances, Compression stockings

Introduction

Graduated compression stockings (GCSs) have been recognized as the mainstay of compression therapy in the prophylaxis, management and treatment of venous disorders of the human lower extremities, such as varicose veins, deep-vein thrombosis, recurrent leg ulcerations, and the control of lymphoedema [1-4]. Immobilization, and prolonged standing and sitting leading to venous stasis and valves malfunction, have been suggested as the principal etiologic factors in the pathogenesis of the aforementioned venous symptoms [5,6].

The medical function of GCSs is to oppose the increased hydrostatic venous pressure and help venous contraction without muscle activity by providing an external and controlled gradient compression and support from the ankle to the thigh for the superficial venous system [7-9]. The greatest pressures are applied at the ankle and gradually decreasing towards the thigh. The amount of pressure required is dependent on the severity of the condition [10,11].

To satisfy the precautionary and therapeutic effectiveness, proper measurements and evaluations of the magnitudes and distributions of the applied skin pressure are a critically important prerequisite. To date, two main experimental approaches have been commonly undertaken. The one mostly used is direct objective pressure testing based on pressure sensors [12-14]. Another commonly used approach is to indirectly estimate pressure performances by testing the physical characteristics of compression materials [14,15], or by calculating pressure values according to the fabric tension based on Laplace's Law [16].

These currently used methods provide the basic tools to quantify and understand the pressure profiles of GCSs. However, certain limitations still exist. At present, there is no testing machine that is able to measure skin pressure over the entire surface of the leg. The introduction of pressure sensors with different dimensions and sensitivities between leg and stocking fabric that would allow changes in the cross-sectional radius of the curvature and subsequently variate the fabric tension over the sensor have been suggested. Meanwhile, these testing modes could not provide the exact reproduction and visualization of the changing pressure profiles in the process of wearing. In addition, the precise mechanisms of action of GCSs remain controversial, if not unclear [1,17,18].

Therefore, we developed a three-dimensional bio-mechanical

*Corresponding author: lively_liurong@yahoo.com

mathematical model for numerically simulating the dynamic pressure functional performances exerted by GCS in pantyhose style, based on the finite element (FE) analysis, and in conjunction with objective pressure testing. This technique will provide a new tool to predict and assess the pressure performances as well as reproduce dynamic interaction between GCS and human leg with reasonable accuracy.

Methods

Development of 3D Geometric Models of Human Leg and GCS

The geometry of the FE leg model was obtained from 3D reconstruction of Magnetic Resonance Imaging (MRI) coronal images from the right leg of a healthy and normal female subject (age 25 years old, height 160 cm, weight 51.40 kg, body mass index 20.07 kg/m^2). To attain the anatomic structures of leg cross-sections, multiple MR images were taken with intervals of 2 mm in the neutral unloaded position (Figure 1(a)). MIMICS v 7.10 (Materialise, Leuven, Belgium) was employed to obtain the boundaries of the skeletons and soft tissues (Figure 1(b)). In the present research stage, a simplified leg model including two principal biological components was developed to simulate the human leg in upright standing position. One component is bones (skeletons)

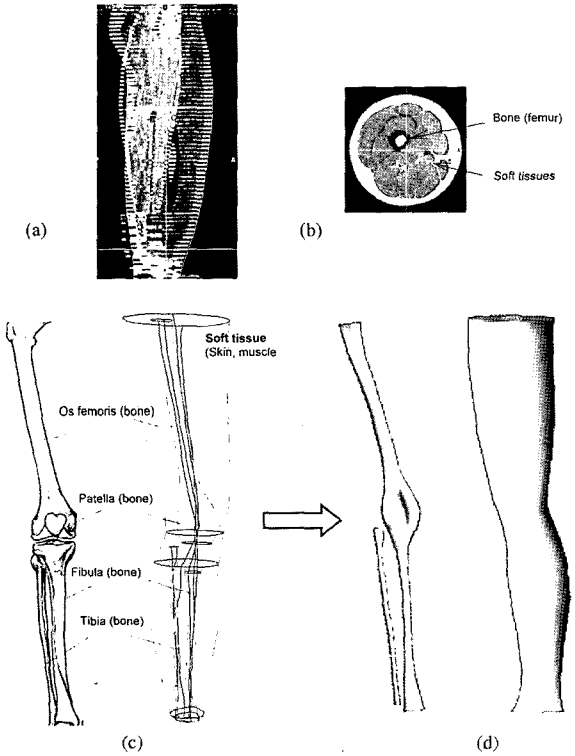

Figure 1. (a) Multiple MRI images of leg with intervals of 2 mm, (b) one cross-section MR image including bone and soft tissue, (c) bone prototype, and (d) simulated solid bones and soft tissue modelling.

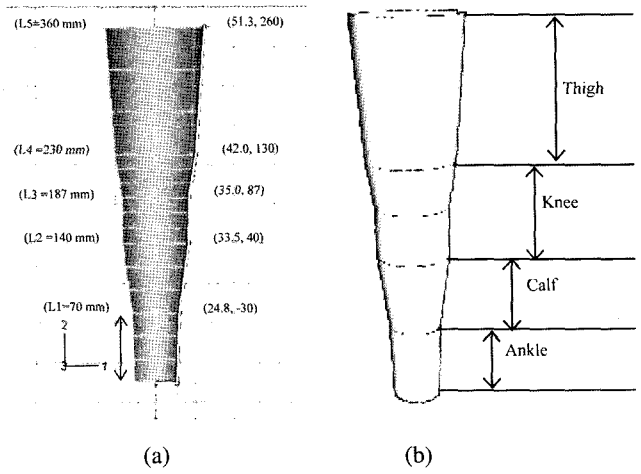

Figure 2. (a) The construction of geometric stocking hose in ABAQUS and (b) 3D digital stocking model with four different parts.

involving the femur, patella, fibula and tibia; another component is soft tissue that is an integration of adipose tissue, skeletal muscle, and skin. The boundary surfaces of the two components were processed by means of Solid Works 2001 (Solid Works Corporation, Massachusetts, US), to create solid models for each bone and soft tissue component (Figure 1(c)-(d)).

The compression stocking for alleviating leg discomfort and preventing varicose veins was used as the geometrical prototype for the simulating stocking hose digital model. The anthropometric estimation of the subject's leg was conducted to identify the fitting size of the GCS. According to the actual stocking size and shape, the 3D digital stocking model was constructed using the FE Package ABAQUS/CAE [19] (Figure 2(a)). The cylindrical stocking hose was divided into four portions (ankle, calf, knee, and thigh) based on actual size in accordance with the "gradient" characteristic of GCS (Figure 2(b)).

Biomaterials and Mechanical Properties of Leg and Stocking Models

The bones including femur, tibia, fibula and patella are taken as rigid and incompressible, and assumed to have no deformations during wearing. The soft tissue is defined as homogeneous, isotropic and linearly elastic biomaterials. The Young's modulus, Poisson's ratio, and mass density of soft tissues are taken as 0.02 MPa, 0.48, and 1.03E-09 tonne/mm^3, respectively [20,21]. The material property of GCS is defined as orthotropic and linearly elastic. Experimentally determined values of fabric parameters were used in the stocking digital modelling. The ratio of stress force to strain on the fabric loading plane along its elongation direction (i.e. Young modulus), was assessed by conducting the strip biaxial tensile testing (KES-G2). The shear modulus reflects

Table 1. Materials properties used in compression stocking modelling

Segments	W (tonne/mm^3)	E_1 (N/mm^2)	E_2 (N/mm^2)	V	G_{12} (N/mm^2)	T (mm)
Ankle	1.3×10^{-10}	0.2778	0.1969	0.2756	0.1741	1
Calf	1.1×10^{-10}	0.2138	0.1500	0.3261	0.1101	1
Knee	0.96×10^{-10}	0.1498	0.1031	0.3766	0.0461	1
Thigh	0.85×10^{-10}	0.1474	0.0957	0.3766	0.0400	1

Illustrate: W: mass density, E_1 and E_2: Young's modulus in the wale and course direction of fabric, V: Poisson's ratio, G_{12}: shear modulus, T: fabric thickness.

the shear rigidity of the GCS fabric, which was estimated with the use of Kawabata evaluation system (KES-FB1 Shear Tester) (Kato-Tec Co., LTD. Japan). Table 1 lists the materials' parameters at different positions along the stocking hose used in the GCS numerical simulation

Numerical Simulation of Mechanical Interaction between Leg and Stocking

Analysis of the Mechanical Interaction Process

During the process of wearing, the interactions between human leg and compression stocking can be differentiated into three fundamental components. The stocking hose is stretched through the human leg, which exerts pressure on the leg surface; and then the pressure compresses the elastic components of the leg and induces the soft tissues to deform and redistribute; and pressure further causes variations of inner tissue stress distributions. Therefore, the surface pressure and inner stress profiles are altered dynamically as the stocking slipped upward from the ankle to the thigh. To simulate the dynamic mechanical interaction between leg and stocking, the kinematical constraints in normal direction and tangent direction of the contact surface need to be formulated.

When it is assumed that the two elastic bodies β^a ($\alpha = 1$, 2), as shown in Figure 3, each occupies the bounded domain $\Omega^a \subset R^3$, the boundary Γ^a of the body β^a consists of three parts: Γ_σ^α with prescribed surface loads, Γ_v^α with prescribed displacements, and Γ_c^α where the two bodies β^1 and β^2 come into contact. There are two cases for the contact condition: non-penetration and a small penetration allowed.

Once the point x^1 of body β^1 in contact with point x^2 of body β^2 is known, we can define an inequality constraint of the non-penetration condition:

$$g_N = (x^2 - x^1) \cdot n^1 \geq 0$$

or a penetration allowed condition:

$$g_N = \begin{cases} (x^2 - x^1) \cdot n^1 & \text{if } (x^2 - x^1) \cdot n^1 < 0 \\ 0 & \text{otherwise} \end{cases}$$

where g_N is the normal gap between the two points. In the tangential direction of the contact interface, one case is

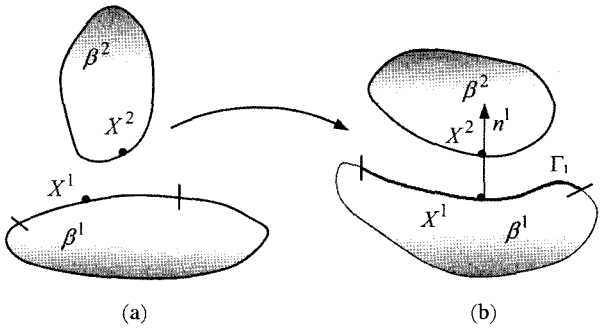

Figure 3. Undeformed and deformed configuration of elastic bodies [22]; (a) undeformed bodies and (b) deformed bodies.

"stick state", in which a point is in contact but not allowed to move in a tangential direction. Another case is "sliding", which means that a point moves in a tangential direction in the contact interface [22]. In the present study, we simulated the interaction between leg and stockings. The two bodies contact and produce sliding and penetration. Penalty method was used for simulating the contact condition.

Numerical Solution with Finite Element Analysis (FEA)

The numerical simulation of interaction between leg and stocking was performed within ABAQUS/CAE (version 6.5) modelling environment with explicit approach. The surface-to-surface contact was applied to simulate the interface interactions between leg and stocking. The friction was assumed to be zero. The two deformable surfaces undergo mechanical finite-sliding and are allowed to arbitrarily move relative to each other forming the contact pair. The penalty contact algorithm is employed to enforce contact constraints between the slave surface nodes (inner surface of stocking hose) and the master surface (leg surface) [19]. Four-node linear tetrahedron solid elements with the global seed size of 8 mm and 4 mm were used for all components of bone, and soft tissues, respectively. For the key cross sections (i.e. ankle, calf, knee, and thigh), the global seed size of 3 mm was employed. The stocking model was meshed with four-node quadrilateral membrane elements and with the global seed size of 3 mm (Figure 4). In the whole putting process, the bones were assumed to be aptotic with the zero displacements of all nodes at x, y, and z directions in the boundary. The top edge

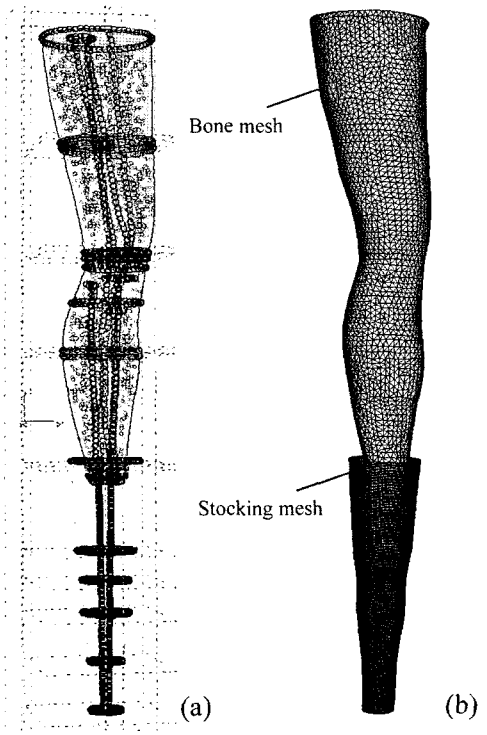

Figure 4. (a) Meshed leg FE model with global seeds at key cross-sections and (b) FM model for simulating dynamic wearing process in mesh.

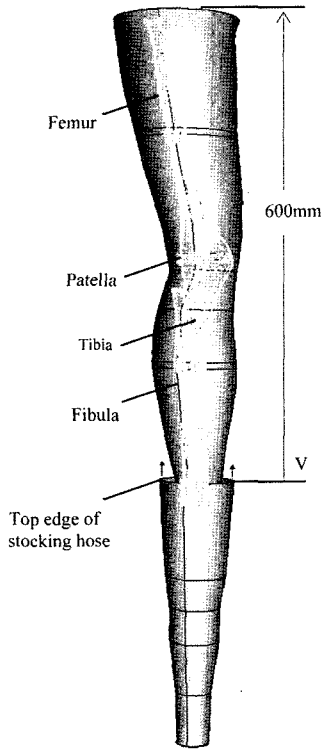

Figure 5. The enactment of boundary condition of bone and stockings in FE model.

of stocking dynamically moves from the distal to the top of the leg in a longitudinal direction with defined displacement (600 mm) and within limited time (10s) (Figure 5). The bottom and the circumferences of the stocking hose can deform freely with hose stretching and the alterations of leg volume.

The Validation of Modelling by Objective Measurements

To validate the developed biomechanical models, the pressure magnitude located at the four different heights (ankle, calf, knee, and thigh), and four different directions (anterior, medial, posterior, and lateral) along the leg applied by GCS were examined using FlexiForce interface pressure sensors (Tekscan, Inc., Boston, MA, USA) and a multichannel monitoring system [7].

Results and Discussion

Longitudinal Pressure and Stress Magnitudes and Distributions

Figure 6(a)-(d) illustrates the simulated magnitude and distribution of leg surface pressure at the anterior side in process of dynamic wearing at 4 sec, 6 sec, 8 sec, and 10 sec, respectively.

It can be seen that as the stocking moved upward from the ankle to the thigh, significant variations in the compression scopes and magnitudes occurred on the leg surface, which was closely related to the stretch states and mechanical function of the covering stocking fabrics. Figure 7(a)-(d) depicts the simulated stress profiles of stocking hose at the corresponding four time points during dynamic wear.

In the few initial seconds (Figure 6(a) and Figure 7(a)), the thigh part of the stocking hose was pulled over the ankle and the calf regions of the leg. Incompletely stretched stocking fabric produced the lower interface pressure at the calf region. When the top edge of the stocking was pulled upward to the thigh (Figure 6(b)-(c) and Figure 7(b)-(c)), more areas of the stocking hose gradually contact with the leg surface, thus producing more stress and multi-dimensional mechanical deformations that included extension, shearing, and bending, which induced more interface pressure generation and spread.

At the end (Figure 6(d) and Figure 7(d)), the greatest stress was found at the areas around the ankle of stocking, followed by the calf. Under the stocking fabric's physical and mechanical actions, gradient pressure was distributed correspondingly along the leg so that the highest compression was exerted at the ankle, and lower compression at the thigh. Since the human leg is a complex irregular cylinder with different surface curvatures, the stocking fabric did not achieve uniform contact everywhere, so that uneven pressure was produced over different parts of the leg.

To describe quantitatively the simulated process of the dynamic interactions between the stocking and leg in wear, sixteen typical nodes located along the ankle, calf, knee and thigh height levels and at the anterior, posterior, lateral and

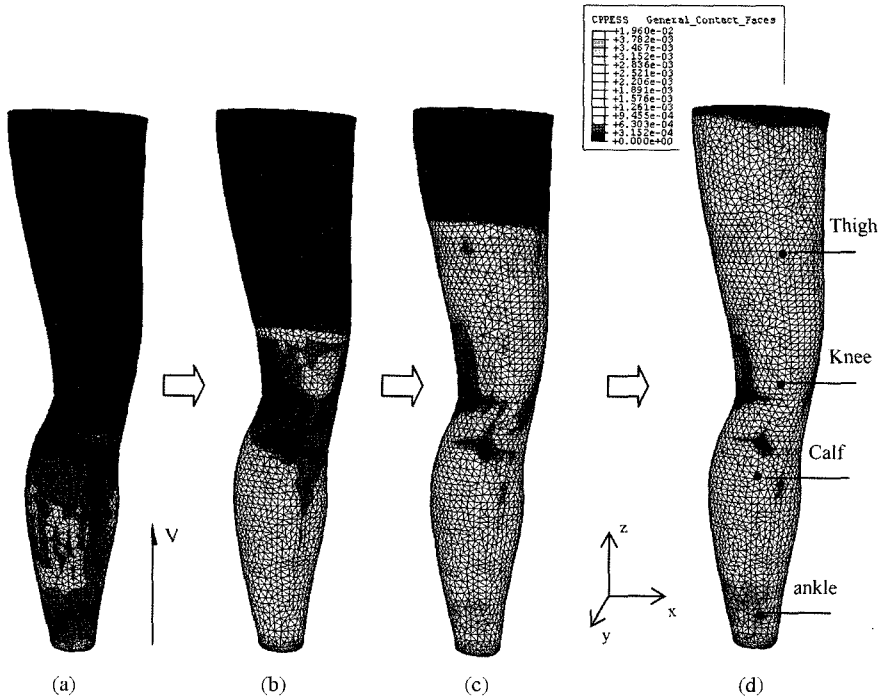

Figure 6. (a) Leg pressure at 4s, (b) leg pressure at 6s, (c) leg pressure at 8s, and (d) leg pressure at 10 s.

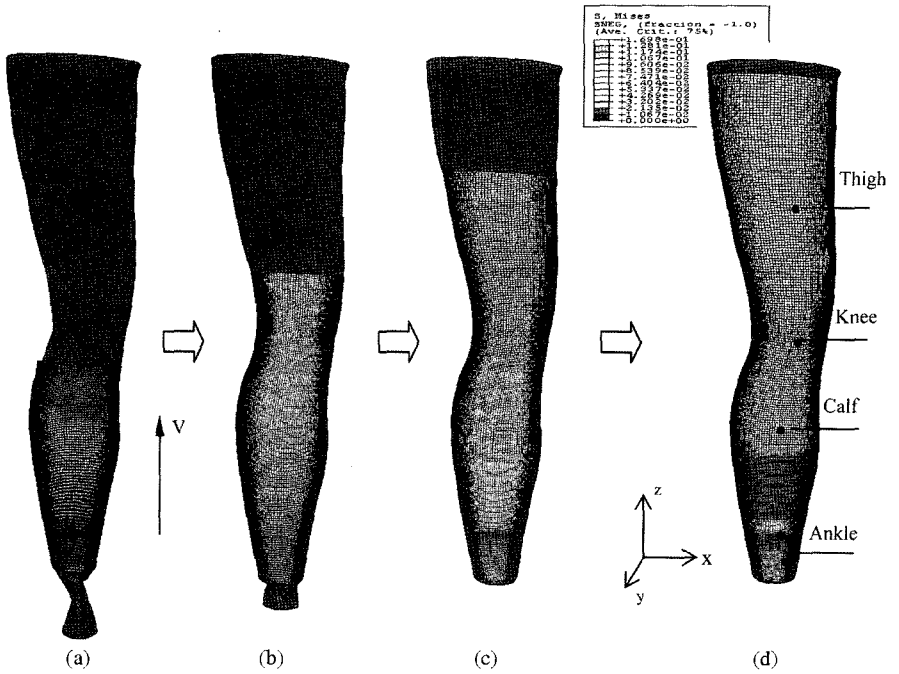

Figure 7. (a) Stocking stress at 4s, (b) stocking stress at 6s, (c) stocking stress at 8s, and (d) stocking stress at 10 s.

medial sides of the leg and stocking respectively was selected (refer to Figure 6(d) and Figure 7(d)). The dynamic alterations of leg pressure and stocking stress at these individual nodes within 10 seconds were presented in Figure 8(a)-(h).

It can be seen from the curve-plots that the magnitudes of pressure and stress all showed marked incremental trends with the time increasing process. Comparing with pressures, stocking stresses produce more significantly smooth, and show increasing trends at the four height levels along stocking hose and on all four sides, especially, starting from the fourth

second in wear (Figure 8(b), (d), (f), and (h)). The stress of the stocking hose was always maintained at higher value at the ankle and calf height levels. On the other hand, the leg pressure curves showed more obvious fluctuations, especially at the anterior, lateral and medial aspects of leg with undulating contact surfaces, and at the ankle and knee height levels owing

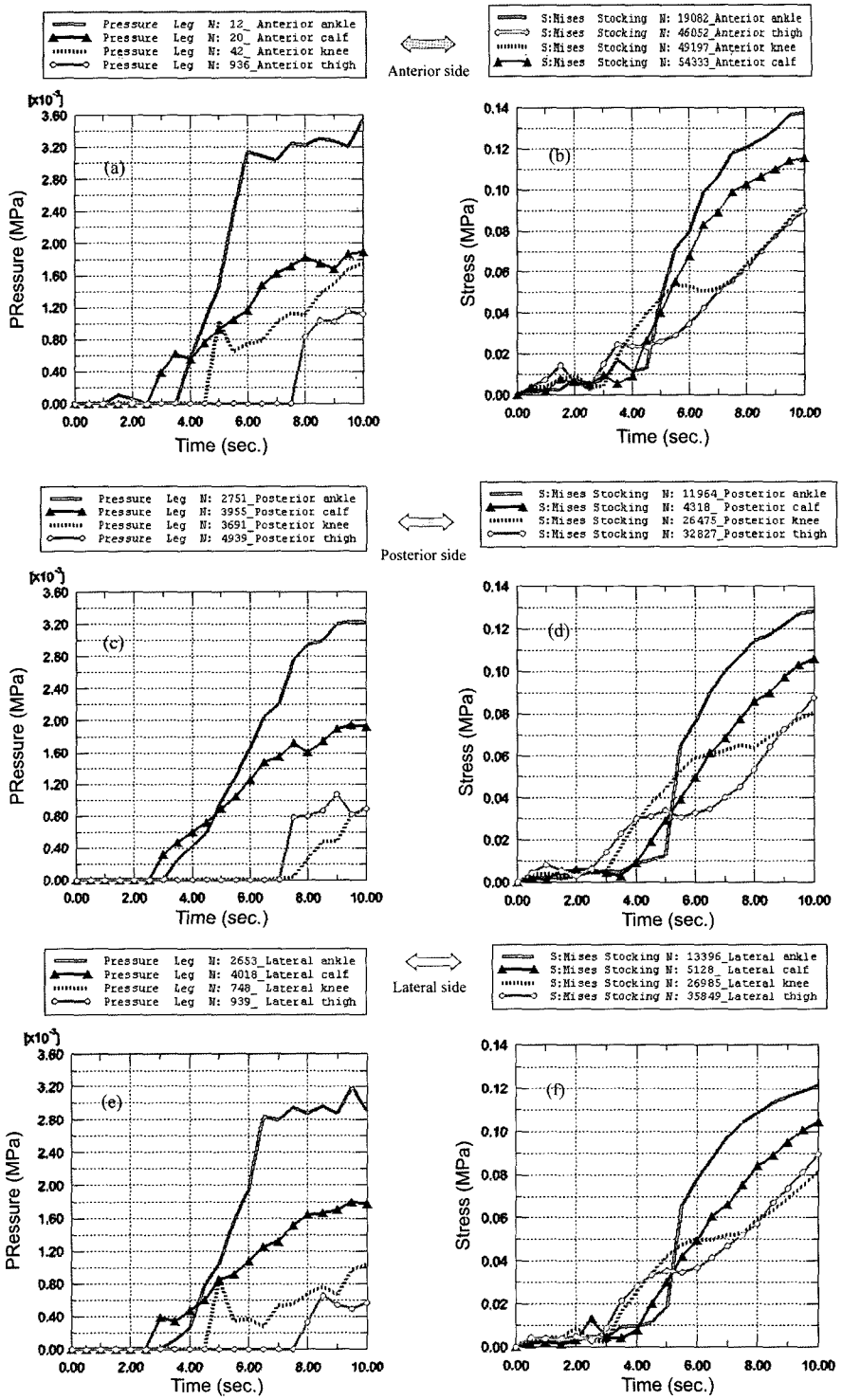

Figure 8-1. (a) Pressure-time curves at anterior side of leg, (b) stress-time curves at anterior side of stocking, (c) pressure-time curves at posterior side of leg, (d) stress-time curves at posterior side of stocking, (e) pressure-time curves at lateral side of leg, and (f) stress-time curves at lateral side of stocking.

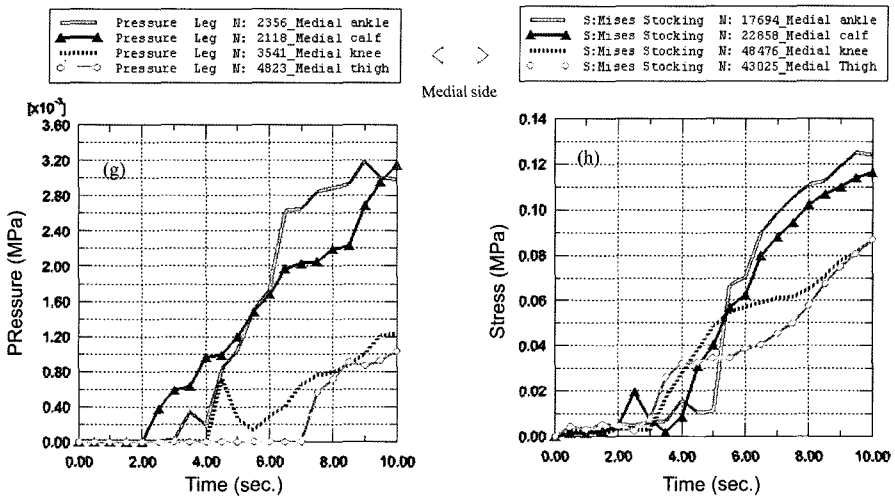

Figure 8-2. (g) Pressure-time curves at medial side of leg and (h) stress-time curves at medial side of stocking.

to their bony structures. Meanwhile, significant differences in pressure magnitudes and alteration patterns occurred among the four height levels of the leg in wear (Figure 8(a), (c), (e), and (g)).

When the stocking hose is pulled over the calf segment at the 4th second, the fabric contacted the leg and became stretched. The stresses at the thigh and the knee regions was first augmented over the four sides, which induced a sharp rise in the corresponding interface pressures at the calf (about 600 Pa-1000 Pa) and the ankle (about 200 Pa-600 Pa), and continued rising trends were maintained. The ankle pressure increased most rapidly in all directions among all height levels. When the whole stocking hose is pulled over the leg at about the 6th second, the ankle pressures attained the first peak values (about 2600 Pa-3100 Pa), especially at the anterior ankle. The first peak value for knee pressure occurred at about the 4.5th-5.0th second when the top edge of the stocking hose was pulled over the patella, especially at the anterior knee with bony prominency. The thigh pressure was last to be produced when the stocking hose was pulled over the thigh area at about the 7.5th second.

Overall, we have observed that the leg pressure profiles were closely related to the changes of stocking stresses. However, the leg pressure magnitudes produced more significant gradient (graded) distributions from the ankle to the thigh regions, and the pressures at different height levels of leg occurred at different periods of time during dynamic wearing. While, the occurrences and alterations of stocking stresses along different height levels appeared more continuously and evenly.

Comparisons between the Simulated and the Measured Results

The female subject who attended leg MRI scan continued to participate in the objective pressure testing. The same GCS was used. The pressure beneath GCS located at the

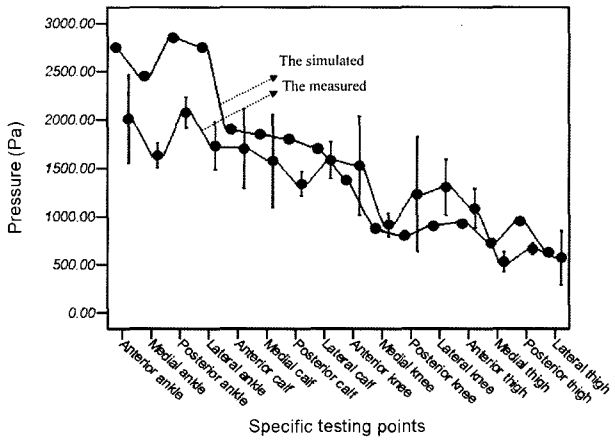

Figure 9. Comparisons on the pressure magnitudes between the simulated and the measured results.

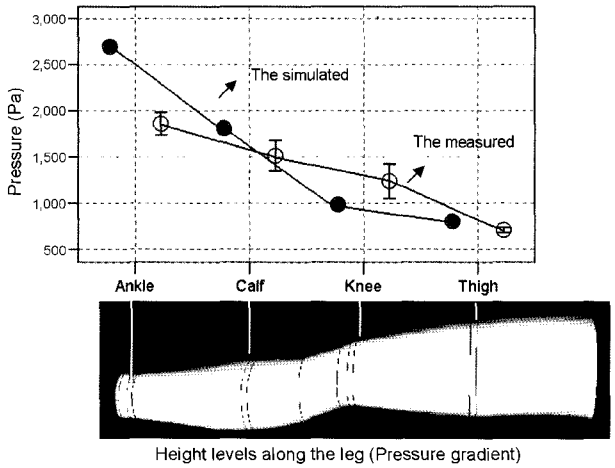

Figure 10. Comparisons on the pressure gradient distributions along the leg among the simulated, the measured, and the advised by the European committee for standardization (i.e. shaded area).

sixteen typical different points when the subject assumed the upright standing position were measured three times. Figure 9 shows the comparison results between the simulated and the measured pressure values.

It can be seen that there was similar changing trends in the pressure magnitudes between the simulated and the measured values. Larger fluctuations in pressure occurred at the ankle and knee regions between the two curves (Figure 9). Although the simulated pressures values at the ankle region were higher than the measured one, their mean value did not exceed the upper limit of ankle range specified by the GCS manufacturers (i.e. 2826 Pa).

Figure 10 shows the comparison results on the pressure gradient distribution proportions among the simulated, the measured, and that recommended by the European committee for standardization (CEN) (i.e. the shaded area). We can see that the simulated (100:67:30) and the measured (100:78:40) pressure gradient distributions at the ankle, calf and thigh regions was in accordance with the corresponding ones recommended by CEN (100:60-80:30-60).

Engineering Design Frame of GCSs Based on Computational Simulation

In this study, the three-dimensional biomechanical model for numerically simulated dynamic interactions between leg-stocking has been developed based on the actual geometries of human leg and compression stockings and in conjunction with wear trials. Figure 11 shows an engineering design frame of GCSs based on the computational simulation methods.

To realize a certain medical function (e.g. to prevent varicose veins), the compression materials with specific mechanical properties and basic structures needed to be designed. Before practical applications, the design parameters can be put into the developed 3D biomechanical mathematical model, to simulate and visualize the practical wearing effect, to help the designer timely find and improve pressure profiles of GCSs. Once the practical product is developed, the skin pressure profiles can be examined by the modelling, thus, quantitatively and qualitatively estimating its medical function

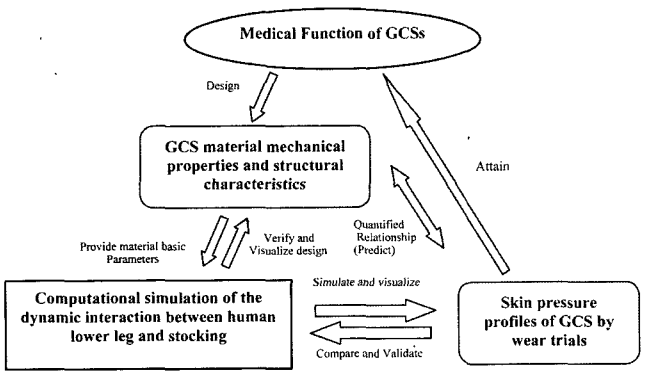

Figure 11. A schematic frame of the engineering design of GCSs based on computational stimulation.

and mechanical performances. The developed quantitative relationships between material properties and pressure profiles can be used as a data reference for the computational simulation and validation.

In this study, the developed FE model demonstrated that the simulated compression stocking hose possessing special material mechanical properties can indeed exert the longitudinal gradient pressure along the leg with the greatest compression at the ankle, which has significant medical function. When a person is standing, owing to the action of gravity, the venous pressure at the ankle region is raised to 80 to 87 mmHg (10,665.8-11,599.0 Pa) [23,24]. For those people, who stand or sit for prolonged periods of time lack of leg muscle activities, the increased hydrostatic pressure will gradually make venous blood pooling in the leg, and the vein valves incompetence. Since the hydrostatic head is gradually reduced from the ankle to the thigh, sufficient and proper external pressure applied to the ankle region is extremely important to oppose the increase in venous pressure and venous insufficiency at the ankle. Meanwhile, the reasonable gradient distribution of pressure applied by stocking also exerts crucial influence to the compression medical efficiencies of GCSs. According to the European committee for standardization (CEN), the GCS with mild pressure (i.e. 15-21 mmHg, or, 1999.8-2799.8 Pa at ankle region) should exert 60-80 % of the ankle pressure at calf region, and 30-60 % of ankle pressure at thigh region. The present simulated pressure gradient from the ankle to the thigh has been demonstrated that agrees with the standard.

In addition, the present simulation results show that the surface pressure distribution along the leg is not uniform, which were closely related to the curvature of cross-sectional contour line and the thickness of underlying tissues. During wearing process, the leg pressure was altered dynamically with the changes of stocking stresses. Both pressure and stress magnitude gradually increased with time. Compared with stress, the leg pressures produced more significant differences among the height levels along the leg, especially between the ankle and the other regions. This simulated result was in agreement with the experimental measurements that had demonstrated that small tension of stocking fabric could induce larger or significant increases in the ankle pressure [25].

We found in this study that although similar changing tendencies occurred between the simulated and the measured curves and within reasonable pressure ranges, some differences still existed, especially at the ankle. This phenomenon may be caused by several factors. In the practical wearing, the stocking is first pulled over the foot. While in the present modelling, the stocking hose was directly pulled over the ankle region. The increased stretching of the bottom fabric when the top edge of the hose was moving up could have brought on more pressure at the ankle-brachia region. In addition, there was no ideal pressure sensor that could monitor

the pressure of the entire leg underneath the stocking. Several individual sensors placed at intervals could not measure the practical pressure exactly, a situation that has been widely acknowledged [26-29]. The measured values were largely dependent on the interface condition, underlying tissues characteristics, and also on the dimension and calibration of transducers utilized. Finally, the biomaterials at different regions along the leg have their individual special mechanical properties (e.g. elasticity, rigid, density, etc). In the present model, we had not allowed different mechanical properties in different tissues. Instead, we assumed a homogenous and linearity soft tissue structure in the analysis.

Conclusion

In this study, through pressure objective testing, material physical estimation and numerical simulation, a new 3D biomechanical mathematical model for numerically simulating the stocking's spacial deformations, the surface pressure magnitude and distribution in longitudinal directions, and dynamic mechanical interactions between human leg-stocking during wear, has been developed and quantitatively analyzed. The simulated model has consistently shown a good agreement with the experimental measurements within reasonable pressure ranges, which provides us a new engineering design approach for the improvement and prediction of pressure functional performances of GCSs products.

Acknowledgements

We would like to thank the Research Grant Council for funding this research through project PolyU 5157/02 E and the Hong Kong Polytechnic University through Projects A188 and YD31.

References

1. M. Hirai, H. Iwata, and N. Hayakawa, *Skin Res. Tech.*, **8**, 236 (2002).
2. B. Belinda, *J. Vasc. Nurs.*, **20**(2), 53 (2002).
3. M. J. Jonker, E. M. De Boer, H. J. Ader, and P. D. Bezemer, *Dermatology*, **203**(4), 294 (2001).
4. R. A. Weiss and D. Duffy, *Dermatol Surg.*, **25**, 701 (1999).
5. J. O. Laurikka, T. Sisto, M. R. Tarkka, O. Auvinen, and M. Hakama, *World Journal of Surgery*, **26**(6), 648 (2002).
6. M. J. Johnson, M. W. Spoule, and J. Paul, *Clin Oncol.*, **11**, 105 (1999).
7. R. Liu, Y. L. Kwok, Y. Li, T. T. Lao, and X. Zhang, *Dermatol Surg.*, **31**, 615 (2005).
8. V. Ibegbuna, K. T. Delis, A. N. Nicolaides, and O. Aina, *J. Vasc. Surg.*, **37**, 420 (2003).
9. P. Lauren, *Good House-keeping*, **233**(1), 41 (2001).
10. J. J. Dale, "Leg Ulcers: Nursing Management-A Research Based Guide", Harrow: Scutari, 1995.
11. J. J. Keachie, "Leg Ulcers: Nursing Management-A Research Based Guide", Harrow: Scutari, 1995.
12. A. Finnie, *Br. J. Nur.*, **9**(6), 8 (2000).
13. R. Stolk, C. P. M. Wegen Van Der-Franken, and H. A. M. Neumann, *Dermatol Surg.*, **30**, 729 (2004).
14. R. Liu, Y. L. Kwok, Y. Li, T. T. Lao, and X. Zhang, *Fibers and Polymers*, **6**(4), 322 (2005).
15. H. Partsch, *Dermatol Surg.*, **31**, 625 (2005).
16. R. Stolk and P. Salz, "Measuring Methods and Standards", Zurich, 1987.
17. T. Benkö, E. A. Cooke, M. A. McNally, and R. A. B. Mollan, *Clin. Orthop.*, **1**, 197 (2001).
18. J. C. J. M. Veraart and H. A. Neumann, *Dermatol Surg.*, **22**, 867 (1996).
19. ABAQUS User's Manual, Version 6.4, "Volume: Prescribed Conditions, Constraints & Interactions", Hibbitt, Karlsson and Sorensen Inc., Pawtucket, USA 21.3.4-1, 2003.
20. H. Walter, "Skeletal Muscle Mechanics", John Wiley & Sons, Ltd., 2000.
21. J. B. Park and R. S. Lakes, "Biomaterials: An Introduction", 2nd ed., Plenum Press, New York and London, 1992.
22. P. Wriggers, "Computational Contact Mechanics", John Wiley & Sons, Ltd., 2002.
23. A. Pollack and E. Wood, *J. Appl. Physiol.*, **1**, 649 (1949).
24. H. Nodeland, R. Ingermansen, R. Reed, and K. Aukland, *Clin. Physiol.*, **3**, 573 (1983).
25. C. J. Wildin, A. C. W. Hui, P. J. Esler, and P. J. Gregg, *BJS.*, **85**, 1228 (1998).
26. M. Clark, *J. Tissue Viabil.*, **4**(2), 3742 (1994).
27. J. Melhuish, D. Wertheim, K. Trenary, R. Williams, and K. Harding, "Proceedings of the 6th European Conference on Advances in Wound Management", Macmillan, London, 1997.
28. R. J. Williams, D. Wertheim, S. Shutler, J. Melhuish, K. Trenary, and K. Harding, "Proceedings of the 6th European Wound Management Association Conference", Macmillan, London, 1997.
29. K. O'Dea and R. Barnett, *European Pressure Ulcer Advisory Panel Review*, **1**(2), 44 (1999).